Warm and cold dark matter in a bouncing universe

Changhong Li*

Department of Astronomy, Key Laboratory of Astroparticle Physics of Yunnan Province, School of Physics and Astronomy, Yunnan University, No.2 Cuihu North Road, Kunming, China 650091

(Received 28 August 2020; accepted 20 November 2020; published 18 December 2020)

Being free of the initial singularity, bouncing cosmology serves as a promising alternative to inflation. However, how entropy production occurs during the postbounce phase is still unclear. In this work, we use a newly identified dark matter (DM) candidate called thermal equilibrium freeze-in DM (EQFIDM), which can directly freeze into thermal equilibrium shortly after a bounce, to trace the entropy-producing decay process of the residual bouncing field (RBF). Specifically, we present a model-independent formalism to obtain all nine possible types of entropy-producing RBF decay within a generic bouncing universe. We show that due to the different types of entropy production, the particle mass of this new DM candidate can range from the sub-keV scale to the super-TeV scale. From current Lyman-α forest observations, we find that although four of the possible types of entropy-producing processes have been excluded, five types remain, suggesting both warm and cold EQFIDM candidates with efficient entropy production mechanisms that are accommodated by the current observations. Then, we illustrate how the nature of the RBF can be constrained by current observations and investigate the potential of EQFIDM to alleviate the small-scale crisis.

DOI: 10.1103/PhysRevD.102.123530

I. INTRODUCTION

As the leading scenario for the early Universe, the theory of inflation solves the horizon and flatness problems and can generate a nearly scale-invariant curvature perturbation that agrees well with current observations of the cosmic microwave background (CMB) [1–4]. However, this theory also inevitably suffers from the initial singularity problem [5]. Due to this concern, bouncing cosmology, which addresses this issue with a nonzero minimum size of the universe, has been extensively studied, such as in [6–23]. As a promising alternative to inflation, bouncing cosmology can also resolve the horizon and flatness problems and generate a nearly scale-invariant curvature spectrum [24–26]. Moreover, a duality has been established between inflation and bounce, indicating that for each inflation model, the corresponding bouncing universe model can generate a curvature perturbation with the same spectral index n_s [27–30]. Therefore, many efforts have been made to concretely distinguish between inflation and bounce based on evidence beyond the CMB spectrum [31–41].

One promising proposal is "big-bounce genesis" [42]. A thermally produced bosonic dark matter (DM) candidate is considered a novel probe for a bouncing universe. It has been shown that in addition to a weakly interacting massive particle (WIMP) candidate [43,44], a nonequilibrium DM (NEQDM) candidate, which belongs to the class of freeze-in DM (FIDM) [45–52], can also be produced in a generic bouncing universe. Due to its tiny cross section, the abundance of NEQDM never reaches thermal equilibrium; consequently, the relic abundance, which is sensitive to cosmic evolution and encodes primordial information, can be used to distinguish the bouncing scenario from inflation.

Encouraged by this finding, the concept of big-bounce genesis has also been applied to fermionic DM candidates [53]. In this context, the WIMP and NEQDM avenues also exist for fermionic candidates. However, there has been no quantitative analysis of a fermionic candidate's thermal decoupling conditions in a bouncing universe, resulting in the omission of the new DM candidate addressed in this paper. More specifically, as demonstrated in [42], the (non) equilibrium conditions and the freeze-out/freeze-in conditions are coincident for bosonic DM candidates, such that only two different thermal production avenues are allowed, i.e., WIMPs and NEQDM. However, for other candidates, such a coincidence may not exist. For instance, by considering a DM candidate with a temperature-independent thermally averaged cross section, a novel avenue between WIMPs and NEQDM has been revealed [54]. Inspired by this, we are motivated to investigate such an avenue for fermionic DM candidates within the bouncing scenario.

Encouragingly, by carefully examining the production and thermal decoupling conditions for fermionic DM candidates within a generic bouncing universe, we reveal such a novel avenue in this paper. Through this avenue, thermal equilibrium freeze-in DM (EQFIDM) particles are

*changhongli@ynu.edu.cn

thermally produced and reach equilibrium at an early time. Shortly after the bounce, these particles directly freeze into equilibrium, with no decrease in abundance. The cross section of EQFIDM can range from the upper bound for NEQDM to the lower bound for WIMPs. As a result, its energy density fraction is proportional to the particle mass, $\Omega_\chi \propto \langle\sigma v\rangle^0 m_\chi$, in contrast to the well-known predictions for WIMPs, $\Omega_\chi^{\rm WIMP} \propto \langle\sigma v\rangle^{-1} m_\chi^0$ [43], and NEQDM, $\Omega_\chi^{\rm NEQDM} \propto \langle\sigma v\rangle m_\chi^2$ [42].

Furthermore, we show that due to its tiny cross section, EQFIDM can freeze into thermal equilibrium at a very early time. In this case, the post-freeze-in entropy production from the residual bouncing field (RBF), which may not be negligible, will eventually affect the relic abundance of EQFIDM. Therefore, we propose to employ EQFIDM to trace such entropy production during the postbounce phase. By presenting a model-independent formalism, we investigate all nine possible types of entropy-producing decay processes of the RBF within a generic bouncing universe and characterize their effects on the EQFIDM abundance. Our results indicate that with different entropy production strengths, the EQFIDM particle mass can range from the sub-keV scale to the super-TeV scale.

From current Lyman-α forest observations of the (non) linear matter spectra [55,56], we find that four of the nine types of entropy-producing processes have already been excluded because of their low entropy production. However, the remaining five types, which suggest warm and cold EQFIDM candidates with more efficient entropy production mechanisms, are accommodated by the current observations. In particular, for one of the five available types, we find that if such an RBF redominates after some duration of freeze-in, the entropy production depends solely on its fundamental nature. Furthermore, we use this case to illustrate how the nature of the RBF can be constrained by current Lyman-α forest observations. Finally, we investigate the potential of EQFIDM to alleviate the well-known small-scale crisis (SSC) [57].

The remainder of this paper consists of four sections. In Sec. II, we demonstrate the EQFIDM avenue by analytically solving the Boltzmann equation for fermionic DM candidates within a generic bouncing universe. Section III presents a model-independent formalism to investigate all nine possible types of entropy production from the RBF and characterize their effects on the EQFIDM abundance. In Sec. IV, we use current Lyman-α forest observations to constrain our results and investigate the potential of EQFIDM to alleviate the SSC. We conclude in the last section.

II. THERMAL EQUILIBRIUM FREEZE-IN DARK MATTER CANDIDATE IN A BOUNCING UNIVERSE

For a thermally produced DM candidate, the evolution of its abundance is governed by the Boltzmann equation,

$$\frac{d(n_\chi a^3)}{a^3 dt} = \widetilde{\langle\sigma v\rangle}[(n_\chi^{\rm eq})^2 - n_\chi^2], \tag{1}$$

where a is the scale factor of the universe; n_χ and $\widetilde{\langle\sigma v\rangle}$ are the number density and thermally averaged cross section, respectively, of the DM particles; and the superscript $^{\rm eq}$ denotes thermal equilibrium.

To analytically solve Eq. (1), we divide the evolution of a generic bouncing universe into five stages, as illustrated in Fig. 1.

(i) The preproduction phase ($T < m_\chi$ & $H < 0$). From the initial low-temperature Bunch-Davies vacuum ($T \simeq 0$), the universe collapses, becoming hotter and, eventually, radiation-dominated [58]. We take $T \simeq m_\chi$ as the end of this phase, thus ensuring that no effective DM production occurs in this phase.

(ii) The contraction phase ($m_\chi \leq T \leq T_b$ & $H < 0$). During this phase, dominated by a cosmic bath, the universe continues to contract. With $T \geq m_\chi$, DM particles are effectively produced (WIMPs and EQFIDM immediately reach thermal equilibrium with a large $\langle\sigma v\rangle$, and NEQDM continues to be produced with a small $\langle\sigma v\rangle$). With further contraction, the universe's background temperature continues to increase until it finally reaches the critical value, $T = T_b \gg m_\chi$, at the end of this phase. Thereafter, the nonstandard-physics-inspired bouncing field becomes dominant and gives rise to bounce.

(iii) The bounce phase ($T \geq T_b$ & $-|H(T_b)| < H < |H(T_b)|$). In this phase, the dominant bouncing field drives the universe to bounce from contraction ($^-$) to expansion ($^+$). Specifically, after the Universe has contracted to its minimum size, it starts to expand. When the background temperature reaches $T = T_b$ during expansion, the cosmic bath becomes

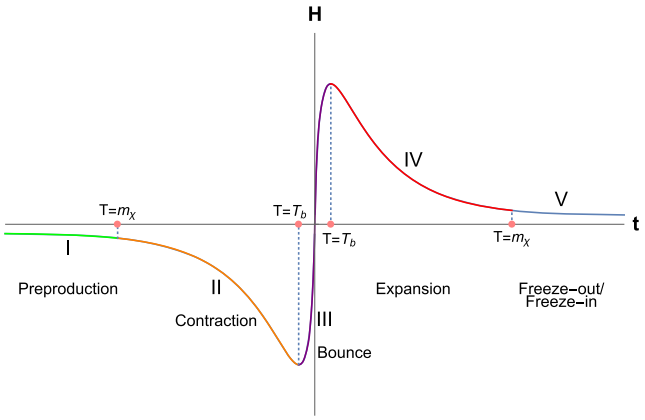

FIG. 1. Hubble parameter vs time. Five stages of DM evolution in a generic bouncing universe, from left to right: I. the preproduction phase (green), II. the contraction phase (orange), III. the bounce phase (purple), IV. the expansion phase (red), and V. the freeze-out/freeze-in phase (blue).

dominant again, and this phase ends. Note that for a robust bounce, the bouncing field is restored. No entropy-producing decay occurs during this phase [58], leading to the matching condition $Y^+(T_b) = Y^-(T_b)$ for WIMPs and EQFIDM [59], where $Y \equiv n_\chi/T^3$ is the DM abundance.

(iv) The expansion phase ($T_b \geq T \geq m_\chi$ & $H > 0$). After the bounce phase, the universe becomes radiation-dominated and continues to expand. As the background temperature falls, the EQFIDM, which has a very tiny cross section, relativistically freezes into thermal equilibrium at a very early time. Meanwhile, the RBF also starts to decay at the beginning of this phase and slightly heats the cosmic bath. If the RBF is depleted after the EQFIDM freezes in, part of its entropy-producing decay will affect the relic abundance of the EQFIDM; therefore, we can use the EQFIDM to trace the RBF. This phase ends at $T = m_\chi$, at which time nonrelativistic thermal decoupling occurs.

(v) The freeze-out/freeze-in phase ($m_\chi > T$ & $H > 0$). In this phase, with nonrelativistic thermal decoupling, WIMPs start to freeze out, and NEQDM starts to freeze in. Note that such nonrelativistic thermal decoupling cannot affect the EQFIDM because the EQFIDM has already relativistically frozen into thermal equilibrium earlier.

According to the above analysis, DM particles are mainly produced in Phase II and Phase IV. In these two phases, we have two scaling relations, $H = \pm H_m y^2$ for the Hubble parameter and $\widetilde{\langle\sigma v\rangle} = \langle\sigma v\rangle y^{-n}$ for the thermally averaged cross section, which can significantly simplify Eq. (1):

$$\frac{dY}{dy} = \mp\kappa y^{-n-2}(1 - \pi^4 g_\chi^{-2} Y^2), \tag{2}$$

where $y \equiv m_\chi/T$; $\kappa \equiv g_\chi^2 \langle\sigma v\rangle m_\chi^3 \pi^{-4} H_m^{-1}$ is a newly introduced dimensionless constant, with g_χ being the number of degrees of freedom of the DM particle and H_m and $\langle\sigma v\rangle$ being constants; and $n = \pm 2$, corresponding to fermions and bosons, respectively [60]. Note that for a bosonic candidate, $n = -2$ leads to coincidence of the equilibrium and freeze-out conditions, so there is no other candidate between WIMPs and NEQDM. This is the reason why EQFIDM has not been identified in the original literature on big-bounce genesis [42]. However, as we will show in this paper, for a fermionic candidate with $n = 2$, there is no such coincidence. Between WIMPs and NEQDM, an EQFIDM avenue exists for fermionic DM candidates in the bouncing universe.

By solving Eq. (2) with the initial condition $Y_-(y = 1) = 0$ [61] and using the matching condition $Y_-(T_b) = Y_+(T_b)$, we can obtain the DM abundance at the end of Phase IV:

$$Y_+(y = 1) = \bar{Y}_\chi^{\rm eq} \tanh\left[\frac{\pi^2}{g_\chi}\frac{2\kappa}{3}\left(\frac{1}{y_b^3} - 1\right)\right], \tag{3}$$

where $\bar{Y}_\chi^{\rm eq} = g_\chi \pi^{-2}$ is the thermal equilibrium abundance in the radiation-dominated phase. The factor of 2 in front of κ reflects that nonequilibrium DM particles can be produced in both the contraction and expansion phases.

By checking whether the DM abundance reaches thermal equilibrium at $y = 1$, we can divide Eq. (3) into two cases:

$$Y_+ = \begin{cases} \bar{Y}_\chi^{\rm eq}, & \tilde{\kappa} \gg 1, \quad \textbf{Equilibrium} \\ \bar{Y}_\chi^{\rm eq}\tilde{\kappa}, & \tilde{\kappa} \ll 1, \quad \textbf{Nonequilibrium} \end{cases}, \tag{4}$$

where $\tilde{\kappa} \equiv \frac{\pi^2}{g_\chi}\frac{2\kappa}{3} y_b^{-3} \propto \langle\sigma v\rangle T_b^3$. This result indicates that for a given value of T_b, only large-cross section DM candidates can reach thermal equilibrium.

As the background temperature falls, nonrelativistic thermal decoupling occurs at $y = 1$. Using $\widetilde{\langle\sigma v\rangle} \to \langle\sigma v\rangle$ and $Y^{\rm eq} \to 0$ in this transition, Eq. (1) can be simplified to

$$\frac{dY}{dy} = -\kappa \frac{\pi^4}{g_\chi^2}\frac{Y^2}{y^2}, \tag{5}$$

for which the solution takes the form

$$Y(y \to \infty) = \left(\frac{3}{2}\frac{\pi^2}{g_\chi} y_b^3 \tilde{\kappa} + Y_+^{-1}\right)^{-1}. \tag{6}$$

Again, this complete solution can be divided into two cases:

$$Y_f = \begin{cases} \tilde{\kappa}^{-1}\frac{2g_\chi}{3\pi^2 y_b^3}, & \tilde{\kappa} \gg Y_+^{-1}\frac{2g_\chi}{3\pi^2 y_b^3}, \quad \textbf{Freeze-out} \\ Y_+, & \tilde{\kappa} \ll Y_+^{-1}\frac{2g_\chi}{3\pi^2 y_b^3}, \quad \textbf{Freeze-in} \end{cases}. \tag{7}$$

Note that these two sets of conditions for (non)equilibrium and freeze-out/freeze-in, Eq. (4) and Eq. (7), are not coincident for fermionic DM candidates, in contrast to the case of bosonic DM candidates [42]. This new observation thus implies that between WIMPs and NEQDM ($1 \ll \tilde{\kappa} \ll \frac{2}{3} y_b^{-3}$), there is a new fermionic candidate (EQFIDM) that undergoes equilibrium production and freeze-in processes, as shown in Fig. 2. To compare all of these three avenues, we use the characteristic relation of the relic energy density fraction, $\Omega_\chi \propto m_\chi Y_f$; our results are presented in Table I. As this table shows, WIMPs have a large cross section, causing them to reach thermal equilibrium and eventually freeze out. NEQDM has such a small cross section that it does not reach thermal equilibrium and, consequently, cannot freeze out. The novel feature of EQFIDM is that its cross section is large enough for it to reach thermal equilibrium but too small for it to freeze

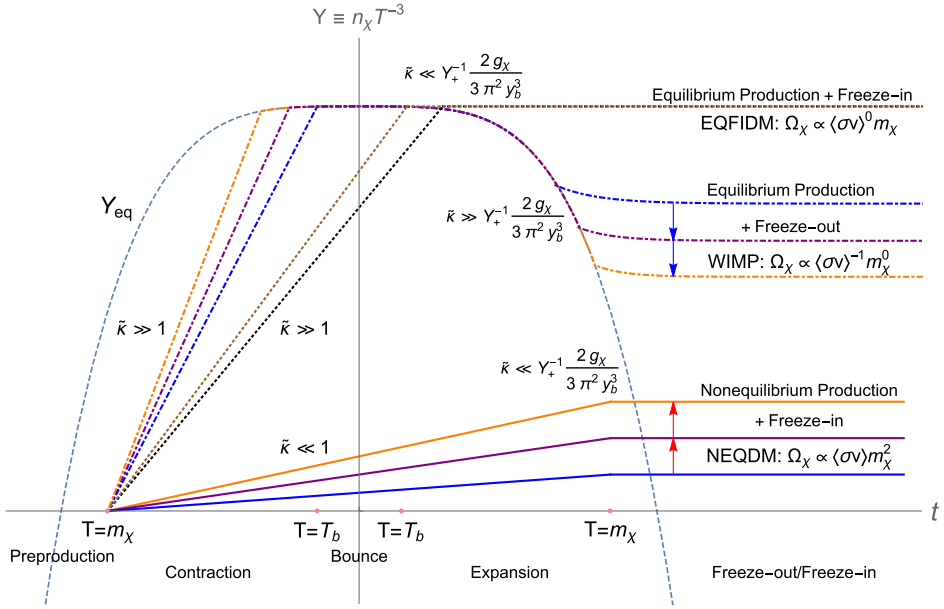

FIG. 2. DM abundance vs time. A schematic plot of the three allowed evolution avenues of thermally produced DM candidates in a generic bouncing universe: WIMPs ($\tilde{\kappa} \gg Y_+^{-1} \frac{2g_\chi}{3\pi^2 y_b^3}$, dot-dashed lines), NEQDM ($\tilde{\kappa} \ll 1$, solid lines) and EQFIDM ($1 \ll \tilde{\kappa} \ll Y_+^{-1} \frac{2g_\chi}{3\pi^2 y_b^3}$, dotted lines), where the value of the dimensionless parameter $\tilde{\kappa} \propto \langle\sigma v\rangle T_b^3$ is determined by the nature of the DM particles and the cosmic background.

out. Hence, it represents an intermediate avenue between WIMPs and NEQDM.

For EQFIDM, by inserting the explicit prefactor into its characteristic relation, we obtain

$$\Omega_\chi = \frac{32.4}{h^2}\left(\frac{g_\chi}{2}\right)\left(\frac{a_{fi}T_{fi}}{a_0 T_0}\right)^3\left(\frac{m_\chi}{1\ \mathrm{keV}}\right), \tag{8}$$

where the subscripts $_{fi}$ and $_0$ denote freeze-in and the present day, respectively. In addition, by applying the condition $1 \ll \tilde{\kappa} \ll \frac{2}{3} y_b^{-3}$, we obtain

$$\frac{3}{2}\frac{\pi^2}{g_\chi}\frac{H_m}{T_b^3} \ll \langle\sigma v\rangle \ll \frac{\pi^2}{g_\chi}\frac{H_m}{m_\chi^3}, \tag{9}$$

which indicates that the EQFIDM cross section can range from the upper bound for NEQDM to the lower bound for WIMPs.

TABLE I. Three avenues in the thermal DM scenario.

	Equilibrium production ($\tilde{\kappa} \gg 1$)	Nonequilibrium production ($\tilde{\kappa} \ll 1$)
Freeze-out $\tilde{\kappa} \gg Y_+^{-1} \frac{2g_\chi}{3\pi^2 y_b^3}$	$\mathcal{A}$: WIMP candidate $\Omega_\chi \propto \langle\sigma v\rangle^{-1} m_\chi^0$	…
Freeze-in $\tilde{\kappa} \ll Y_+^{-1} \frac{2g_\chi}{3\pi^2 y_b^3}$	$\mathcal{C}$: EQFIDM candidate $\Omega_\chi \propto \langle\sigma v\rangle^0 m_\chi$	$\mathcal{B}$: NEQDM candidate $\Omega_\chi \propto \langle\sigma v\rangle m_\chi^2$

According to Eq. (8), Ω_χ is determined not only by m_χ but also by the factor $(a_{fi}T_{fi}/a_0T_0)^3$. Therefore, EQFIDM candidates with different $\langle\sigma v\rangle$ may have different Ω_χ. The reason is that the value of $(a_{fi}T_{fi}/a_0T_0)^3$ depends on the magnitude of the post-freeze-in entropy production. Because EQFIDM candidates with different $\langle\sigma v\rangle$ freeze into thermal equilibrium at different times, they may have different $(a_{fi}T_{fi}/a_0T_0)^3$, resulting in different Ω_χ. For instance, in the large $\langle\sigma v\rangle$ limit, $\langle\sigma v\rangle \to \frac{\pi^2}{g_\chi}\frac{H_m}{m_\chi^3}$, the EQFIDM can track thermal equilibrium for a very long time and finally freeze into thermal equilibrium at very late time, $T_{fi} \simeq m_\chi$; consequently, only very little entropy can be produced after freeze-in, and $(a_{fi}T_{fi}/a_0T_0)^3 \simeq 1$. On the other hand, in the small $\langle\sigma v\rangle$ limit, $\langle\sigma v\rangle \to \frac{3}{2}\frac{\pi^2}{g_\chi}\frac{H_m}{T_b^3}$, the EQFIDM will track thermal equilibrium for only a very short time and then freeze into thermal equilibrium much earlier, at $T_{fi} \simeq T_b$. In this case, the post-freeze-in entropy production could be very large, and $(a_{fi}T_{fi}/a_0T_0)^3 \ll 1$.

In this paper, we mainly consider two general entropy-producing processes, one from the annihilation of Standard Model (SM) particles and one from RBF decay. Without loss of generality, we can take $T_r \sim 100$ GeV to separate these two entropy-producing processes [62]:

$$\left(\frac{a_{fi}T_{fi}}{a_0T_0}\right)^3 = \left(\frac{a_{fi}T_{fi}}{a_rT_r}\right)^3\left(\frac{a_rT_r}{a_0T_0}\right)^3. \tag{10}$$

By doing so, we can divide EQFIDM candidates into three categories:

(i) Large $\langle\sigma v\rangle$. For a large cross section ($T_{fi} \ll T_r$), the EQFIDM will freeze into thermal equilibrium at a very late time, so no entropy is produced after freeze-in, $(a_{fi}T_{fi}/a_0T_0)^3 \simeq 1$. By substituting this relation into Eq. (8), we obtain

$$m_\chi = 0.004 \text{ keV}, \tag{11}$$

where we have used $\Omega_\chi \simeq 0.26$ and $g_\chi = 2$. Obviously, such a hot DM candidate is not favored by current astrophysical observations [63].

(ii) Moderate $\langle\sigma v\rangle$. For a moderate cross section ($T_{fi} \sim T_r$), the EQFIDM will freeze into thermal equilibrium after the entropy-producing decay of the RBF but before SM particle annihilations. Therefore, we have $(a_{fi}T_{fi}/a_rT_r)^3 = 1$ and $(a_rT_r/a_0T_0)^3 \simeq 1/30$ [63], yielding

$$m_\chi = (\Omega_\chi/2.2) \text{ keV}. \tag{12}$$

Note that this prediction is degenerate with the prediction in the case of inflation. The reason is that without the entropy-producing decay of the RBF, the EQFIDM will freeze into the same equilibrium background in both the bouncing and inflation scenarios. In particular, for $\Omega_\chi = 0.26$, we have $m_\chi \simeq 0.1$ keV, which is still not a good fermionic DM candidate because it is incompatible with the condition for forming fermionic DM halos ($m_\chi \geq 0.48$ keV) [64].

(iii) Small $\langle\sigma v\rangle$. For a small cross section ($T_{fi} \gg T_r$), the EQFIDM will freeze into thermal equilibrium in a very early epoch and thus can trace part of the entropy-producing decay of the RBF; accordingly, we have

$$m_\chi = \xi^{-1} \times (\Omega_\chi/2.2) \text{ keV}, \tag{13}$$

where $\xi \equiv (a_{fi}^3 s_{fi}/a_r^3 s_r) = (a_{fi}T_{fi}/a_rT_r)^3$ is introduced, with $s = \frac{2\pi^2}{45} g_\star T^3$ being the background entropy density and $g_\star$ being the number of background degrees of freedom. As shown in the next section, for an effective entropy-producing RBF decay, ξ can be much smaller than 1, and the particle mass of the EQFIDM can be several orders of magnitude higher than 0.1 keV, thereby resolving the aforementioned tensions.

In the next section, we will focus on the small $\langle\sigma v\rangle$ case to compute ξ for all possible entropy-producing decay processes of the RBF.

III. THE ENTROPY-PRODUCING DECAY OF THE RESIDUAL BOUNCING FIELD

After bounce, the residual part of the bouncing field, such as quintom matter [65], starts to decay and slightly heats the cosmic bath. Without loss of generality, we take $\Gamma_\star$ to be the effective dissipative constant for such a decay. Thus, the equations of motion governing the entropy-producing decay of the RBF take the following forms:

$$\frac{d\rho_b}{dt} + 3(1+w_b)H\rho_b = -\Gamma_\star \rho_b, \tag{14}$$

$$\frac{d(sa^3)^{\frac{4}{3}}}{dt} = \frac{4}{3}\left(\frac{2\pi^2}{45} g_\star\right)^{\frac{1}{3}} \Gamma_\star \rho_b a^4, \tag{15}$$

and

$$H^2 = \frac{1}{3M_p^2}(\rho_b + \rho_\gamma), \tag{16}$$

where ρ_γ is the total energy density of the cosmic bath, ρ_b is the energy density of the RBF, and $w_b \equiv p_b/\rho_b$ is the equation of state (EoS). Following [66], we have used $a^{-4}d(\rho_\gamma a^4)/dt = \Gamma_\star \rho_b$ with $s = \frac{2\pi^2}{45} g_\star T^3$ and have ignored the variation in $g_\star$ during the process of interest (i.e., we have assumed $dg_\star/dt = 0$) to derive Eq. (15).

Substituting the solution of Eq. (14), $\rho_b(t) = \rho_b(t_{fi})(\frac{a(t)}{a(t_{fi})})^{-3(1+w_b)} e^{-\Gamma_\star(t-t_{fi})}$, into Eq. (15) and integrating it, we obtain

$$\xi = [I+1]^{-\frac{3}{4}}, \tag{17}$$

where the newly introduced dimensionless parameter takes the form

$$I = \epsilon \int_{t_{fi}}^{t_r} \Gamma_\star e^{-\Gamma_\star(t-t_{fi})} \left(\frac{a(t)}{a(t_{fi})}\right)^{(1-3w_b)} dt, \tag{18}$$

with $\epsilon \equiv \rho_b(t_{fi})/\rho_\gamma(t_{fi})$ being the ratio of the energy density of the RBF to that of the cosmic bath at $T = T_{fi}$. By substituting Eq. (17) into Eq. (13), we obtain

$$m_\chi = [I+1]^{\frac{3}{4}} \times (\Omega_\chi/2.2) \text{ keV}, \tag{19}$$

which implies that for a given value of Ω_χ, an effective post-freeze-in entropy production process ($I \gg 1$) can result in a large m_χ for EQFIDM.

$\Gamma_\star$ and w_b, which reflect the fundamental nature of the RBF, and ϵ are all model-dependent quantities in various realizations of the bouncing cosmos. Therefore, in this paper, we are motivated to perform a model-independent analysis to include all possibilities. As follows, using ϵ and I, the entropy-producing decay processes of the RBF

within a generic bouncing universe can be categorized into three cases: A. subdominant entropy production ($\epsilon \ll 1$ and $I \ll 1$), B. dominant entropy production ($\epsilon \gg 1$), and C. redominant entropy production ($\epsilon \ll 1$ and $I \geq 1$).

A. Subdominant entropy production ($\epsilon \ll 1$ and $I \ll 1$)

For the subdominant case, $\epsilon \ll 1$, and the RBF is assumed to always be subdominant ($\rho_b \ll \rho_\gamma$) since $T = T_{fi}$. Thus, entropy production occurs against a purely radiation-dominated background, and the solution to Eq. (16) takes the form

$$a = a(t_{fi})[2H(t_{fi})(t - t_{fi}) + 1]^{\frac{1}{2}}. \tag{20}$$

By substituting this expression into Eq. (18), we obtain

$$I = \epsilon \int_{t_{fi}}^{t_r} \Gamma_\star e^{-\Gamma_\star (t-t_{fi})} [2H(t_{fi})(t-t_{fi})+1]^{\frac{1}{2}(1-3w_b)} dt. \tag{21}$$

As listed in Table II, using the condition $\Gamma_\star = 2H(t_{fi})$ and $w_b = \frac{1}{3}$, this integral can be further divided into four subcases, corresponding to four types of subdominant entropy-producing decay processes. In particular, for the types with large $\Gamma_\star$ (Type 3 and Type 4), the decay process is so swift that the redshift can be neglected. Thus, we obtain $I = \epsilon$, which is independent of w_b and $\Gamma_\star$, and find that the entropy production for Type 3 and Type 4 is negligible because $\epsilon \ll 1$. On the other hand, for the types with small $\Gamma_\star$ (Type 1 and Type 2), the entropy production occurs over a longer period and the redshift should be taken into account, leading to

TABLE II. Subdominant entropy production ($\epsilon \ll 1$ and $I \ll 1$).

	Small w_b $(-1 \leq w_b \leq \frac{1}{3})$	Large w_b $(\frac{1}{3} \leq w_b \leq 1)$
Small $\Gamma_\star$	Type 1: $(\Gamma_\star \gg 2H(t_{fi})[\epsilon^{-\frac{2}{1-3w_b}} - 1]^{-1})$	Type 2
$\Gamma_\star < 2H(t_{fi})$	$\epsilon \leq I \ll 1$	$I < \epsilon \ll 1$
Large $\Gamma_\star$	Type 3	Type 4
$\Gamma_\star > 2H(t_{fi})$	$I = \epsilon \ll 1$	$I = \epsilon \ll 1$

$$I = \begin{cases} \epsilon \times \left(\frac{2H(t_{fi})}{\Gamma_\star}\right)^{\frac{1}{2}(1-3w_b)} e^{\frac{\Gamma_\star}{2H(t_{fi})}} \Gamma\left[\frac{3}{2}(1-w_b), \frac{\Gamma_\star}{2H(t_{fi})}\right] \geq \epsilon, & w_b \leq \frac{1}{3} \\ \epsilon \times \int_0^\infty \left(\frac{2H(t_{fi})}{\Gamma_\star} x + 1\right)^{\frac{1}{2}(1-3w_b)} e^{-x} dx < \epsilon, & w_b > \frac{1}{3} \end{cases}, \tag{22}$$

where $\Gamma[a,x] \equiv \int_x^\infty t^{a-1} e^{-t} dt$ is the incomplete Gamma function. For Type 2, the RBF with $w_b > \frac{1}{3}$ is strongly redshifted, so its entropy production is negligible, $I \ll \epsilon \ll 1$. For Type 1, because $w_b \leq \frac{1}{3}$, entropy production occurs over a longer time, such that $I \geq \epsilon$. However, the subdominant condition requires $\Gamma_\star \gg 2H(t_{fi})[\epsilon^{-\frac{2}{1-3w_b}} - 1]^{-1}$, which implies that $I \ll 1$ (see the Appendix). Consequently, the entropy production for Type 1 is also negligible. In short, we can conclude that in the subdominant case, regardless of the values of $\Gamma_\star$ and w_b, the entropy production is always negligible. In particular, for $\Omega_\chi = 0.26$, the EQFIDM particle mass is $m_\chi \simeq 0.1$ keV for these four decay types.

B. Dominant entropy production ($\epsilon \gg 1$)

Although the cosmic bath dominates at the end of the bounce phase ($T = T_b$), as the expansion phase proceeds, an RBF with a smaller w_b has the possibility of becoming dominant again for some time. If the EQFIDM freezes into thermal equilibrium in such an RBF-dominated era, we have $\epsilon > 1$, and the solution to Eq. (16) takes the form

$$a(t) = a(t_{fi}) \left[\frac{3(1+w_b)}{2} \frac{2H(t_{fi})}{\Gamma_\star} (1 - e^{-\frac{\Gamma_\star}{2}(t-t_{fi})}) + 1\right]^{\frac{2}{3(1+w_b)}}. \tag{23}$$

By substituting this expression into Eq. (18), we obtain

$$I = \epsilon \int_{t_{fi}}^{t_r} \Gamma_\star \left[\frac{3(1+w_b)}{2} \frac{2H(t_{fi})}{\Gamma_\star} (1 - e^{-\frac{\Gamma_\star}{2}(t-t_{fi})}) + 1\right]^{\frac{2(1-3w_b)}{3(1+w_b)}} \times e^{-\Gamma_\star (t-t_{fi})} dt. \tag{24}$$

As listed in Table III, using $\Gamma_\star = 2H(t_{fi})$ and $w_b = \frac{1}{3}$, such dominant entropy-producing decay processes can also be categorized into four types. For Type 7 and Type 8, a large $\Gamma_\star$ makes the redshift effect negligible, leading to $I = \epsilon$. Because $\epsilon \gg 1$ in this case, efficient entropy production occurs in processes of Type 7 and Type 8. On the other hand, for the types with small $\Gamma_\star$ (Type 5 and Type 6), by considering the redshift effect, we obtain

TABLE III. Dominant entropy production ($\epsilon \gg 1$).

	Small w_b $(-1 < w_b \leq \frac{1}{3})$	Large w_b $(\frac{1}{3} < w_b \leq 1)$
Small $\Gamma_\star$ $\Gamma_\star < 2H(t_{fi})$	Type 5 $I = \epsilon \frac{\left(\frac{\Gamma_\star}{2H(t_{fi})}+\frac{3(1+w_b)}{2}\right)^2}{(5-3w_b)}\left(1+\frac{3(1+w_b)}{2}\frac{2H(t_{fi})}{\Gamma_\star}\right)^{\frac{2(1-3w_b)}{3(1+w_b)}}$ $\geq \epsilon \gg 1$	Type 6 $I = \epsilon \frac{\left(\frac{\Gamma_\star}{2H(t_{fi})}+\frac{3(1+w_b)}{2}\right)^2}{(5-3w_b)}\left(1+\frac{3(1+w_b)}{2}\frac{2H(t_{fi})}{\Gamma_\star}\right)^{\frac{2(1-3w_b)}{3(1+w_b)}}$ $< \epsilon$
Large $\Gamma_\star$ $\Gamma_\star > 2H(t_{fi})$	Type 7 $I = \epsilon \gg 1$	Type 8 $I = \epsilon \gg 1$

$$I = \epsilon \frac{\left(\frac{\Gamma_\star}{2H(t_{fi})}+\frac{3(1+w_b)}{2}\right)^2}{(5-3w_b)}\left(1+\frac{3(1+w_b)}{2}\frac{2H(t_{fi})}{\Gamma_\star}\right)^{\frac{2(1-3w_b)}{3(1+w_b)}}. \tag{25}$$

For Type 5, because $w_b \leq \frac{1}{3}$, the RBF is redshifted more slowly than the cosmic bath, so the entropy production is very efficient, $I \geq \epsilon \gg 1$. However, for Type 6 with $w_b > \frac{1}{3}$, the RBF is redshifted faster than the cosmic bath, so the entropy production is diluted, $I \leq \epsilon$. In summary, the entropy production in decays of Type 7, Type 8, and Type 5 is very efficient, and we have $m_\chi \gg 0.1$ keV for these decay types. By contrast, for Type 6, because $0 \leq I \leq \epsilon$, m_χ ranges from 0.1 keV to $\epsilon^{\frac{3}{4}} \times 0.1$ keV for different values of w_b and $\Gamma_\star$.

C. Redominant entropy production ($\epsilon \ll 1$ and $I \geq 1$)

In the redominant case, we again have $\epsilon \ll 1$ and $\Gamma_\star < 2H(t_{fi})$, the same as for Type 1 decays in the subdominant case. However, we will now investigate the other part of the parameter region, $\Gamma_\star \ll 2H(t_{fi})[\epsilon^{-\frac{2}{1-3w_b}} - 1]^{-1}$, which allows the RBF to become redominant after the EQFIDM freezes in. To facilitate our analysis, we divide the history for this kind of process into three phases:

(1) The pre-redominant phase ($t_{fi} \leq t \leq t_{rd}$). The RBF is subdominant, so the entropy production is negligible.
(2) The redominant phase ($t_{rd} \leq t \leq t_{rsd}$). The RBF becomes redominant, resulting in efficient entropy production.
(3) The post-redominant phase ($t > t_{rsd}$). As the RBF is depleted, the cosmic bath becomes dominant again, so the entropy production is again negligible.

Here, $t_{rd} = [2H(t_{fi})]^{-1}(\epsilon^{-\frac{2}{1-3w_b}} - 1)$ can be obtained from $\rho_\gamma(t_{rd}) = \rho_b(t_{rd})$, and $t_{rsd} \to \infty$ can be assumed for simplicity.

Because the main contribution to entropy production occurs in the redominant phase, we have

$$I = \epsilon \frac{\rho_b(t_{rd})}{\rho_b(t_{fi})}\left(\frac{a(t_{rd})}{a(t_{fi})}\right)^4 \int_{t_{rd}}^{t_{rsd}} \Gamma_\star \frac{\rho_b}{\rho_b(t_{rd})}\left(\frac{a}{a(t_{rd})}\right)^4 dt. \tag{26}$$

By calculating the integral with the background solution,

$$a(t) = a(t_{rd})\left[\frac{3(1+w_b)}{2}\frac{2H(t_{fi})}{\Gamma_\star}(1 - e^{-\frac{\Gamma_\star}{2}(t-t_{fi})}) + 1\right]^{\frac{2}{3(1+w_b)}}, \tag{27}$$

and using $\frac{\rho_b(t_{rd})}{\rho_b(t_{fi})}(\frac{a(t_{rd})}{a(t_{fi})})^4 = \epsilon^{-1}$ (see the Appendix), we obtain

$$I = \frac{(\frac{\Gamma_\star}{2H(t_{fi})} + \frac{3(1+w_b)}{2})^2}{(5-3w_b)}\left(1+\frac{3(1+w_b)}{2}\frac{2H(t_{fi})}{\Gamma_\star}\right)^{\frac{2(1-3w_b)}{3(1+w_b)}}, \tag{28}$$

which is independent of ϵ (note that this result is different from that for Type 5 by a factor of ϵ). Notably, this result implies that if the RBF can become redominant, its entropy production depends solely on its fundamental nature, as reflected by $\Gamma_\star/2H(t_{fi})$ and w_b. This is because the main contribution to entropy production occurs during the redominant phase ($t_{rd} \leq t \leq t_{rsd}$), for which the duration and other details depend only on $\Gamma_\star/2H(t_{fi})$ and w_b. In other words, for a sufficiently small $\Gamma_\star$, $\Gamma_\star \ll 2H(t_{fi})[\epsilon^{-\frac{2}{1-3w_b}} - 1]^{-1}$, the decay of the RBF can still lead to a significant contribution to the post-freeze-in entropy production even if the RBF contributes only a very small portion of the total energy density at freeze-in.

In Table IV, we list the characteristics of Type 9 entropy-producing decay. As we will show, for different values of $\Gamma_\star/2H(t_{fi})$ and w_b, the EQFIDM particle mass corresponding to this decay type can range from the sub-keV scale to the super-TeV scale.

In summary, by performing a model-independent analysis of the entropy-producing decay of the RBF within a generic bouncing universe, we have identified all three general cases of entropy production, which can be subdivided into nine different types. Specifically, the entropy

TABLE IV. Redominant entropy production ($\epsilon \ll 1$ and $I \geq 1$).

	Small w_b $(-1 < w_b \leq \frac{1}{3})$	Large w_b $(\frac{1}{3} \leq w_b \leq 1)$
Small $\Gamma_\star$ $\Gamma_\star < 2H(t_{fi})$	Type 9: $(\Gamma_\star \ll 2H(t_{fi})[\epsilon^{-\frac{2}{1-3w_b}} - 1]^{-1})$ $I = \frac{\left(\frac{\Gamma_\star}{2H(t_{fi})} + \frac{3(1+w_b)}{2}\right)^2}{(5-3w_b)} \left(1 + \frac{3(1+w_b)}{2}\frac{2H(t_{fi})}{\Gamma_\star}\right)^{\frac{2(1-3w_b)}{3(1+w_b)}}$	…
Large $\Gamma_\star$	…	…

production in processes of Type 5, Type 7, and Type 8 is very efficient, leading to $m_\chi \gg 0.1$ keV. In processes of Type 1, Type 2, Type 3, and Type 4, the entropy production is inefficient, so $m_\chi \simeq 0.1$ keV. For Type 6, because the entropy production can be diluted by the redshift effect, $0.1 \text{ keV} \leq m_\chi \ll \epsilon^{\frac{3}{4}} \times 0.1$ keV. Finally, in the most interesting case, Type 9, the entropy production is determined solely by the fundamental nature of the RBF, as reflected by $\Gamma_\star/2H(t_{fi})$ and w_b, and is independent of ϵ. With different values of $\Gamma_\star/2H(t_{fi})$ and w_b, the EQFIDM particle mass can range from the sub-keV scale to the super-TeV scale. In the next section, we will investigate how current astrophysical observations can constrain the possible types of entropy production.

IV. ASTROPHYSICAL IMPLICATIONS

Because EQFIDM consists of collisionless particles, its motion can smooth out inhomogeneities of spacetime and matter during late-time evolution and induce a suppression of the linear matter spectrum at a scale comparable to its free-streaming length [67],

$$L_{fs} \simeq 0.11 \left(\frac{\Omega_\chi h^2}{0.15}\right)^{\frac{1}{3}} \left(\frac{m_\chi}{\text{keV}}\right)^{-\frac{4}{3}} \text{Mpc} = 1.8(I+1)^{-1} \text{ Mpc}, \tag{29}$$

where Eq. (13) and Eq. (17) have been used in the last step. According to this equation, with inefficient entropy production ($I \leq 1$), this suppression occurs on a scale of approximately $L_{\text{fs}} \simeq 1.8$ Mpc, which is too large to be compatible with the current Lyman-α forest observations of the (non)linear matter spectrum—as we will show. Only if the entropy production from the RBF is efficient ($I \gg 1$) can the suppression scale be as small as desired.

To explicitly plot the linear matter spectrum in the presence of EQFIDM, we adopt the numerical simulation results presented in Ref. [56]. Due to the free streaming of the EQFIDM, the linear matter spectrum takes the form

$$P(k) = P_{\text{cdm}}(k)\mathcal{T}^2(k), \tag{30}$$

where $P_{\text{cdm}}(k)$ is the spectrum corresponding to the extreme cold DM (CDM) candidate and $\mathcal{T} = [1 + (\alpha k)^{2\nu}]^{-\frac{5}{\nu}}$ is a transfer function with $\nu = 1.12$ and $\alpha = 0.57(\frac{\Omega_\chi}{0.26})(I+1)^{-0.83}$.

In Fig. 3, we plot the linear matter spectrum for EQFIDM with $I = \{10^{-2}, 10, 50, 300\}$ (the dotted lines from left to right), a warm DM candidate with $m_\chi = 5.3$ keV (the dashed line), and the fiducial CDM candidate ($m_\chi \to \infty$, the solid line) to illustrate how the cut in the spectrum depends on the value of I. The results show that for a larger I, the suppression of the spectrum occurs on a

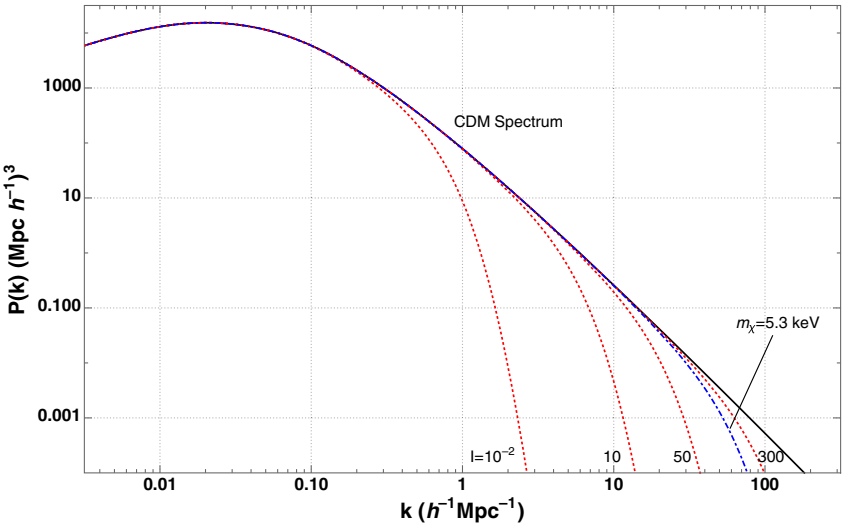

FIG. 3. Power spectra of linear matter perturbations for EQFIDM with $I = \{10^{-2}, 10, 50, 300\}$ (the dotted lines from left to right), a warm DM candidate with $m_\chi = 5.3$ keV (the dashed line), and the fiducial CDM candidate (the solid line).

smaller scale because a heavier EQFIDM mass corresponds to a shorter free-streaming length. Note that these are only the theoretical curves of the linear matter spectrum. In astrophysical observations, at low redshifts ($z \simeq 0$), the linear matter spectrum is not valid for $k \geq 0.1h$ Mpc^{-1} because nonlinear clustering effects are no longer negligible (see [68] for a review). Consequently, the Lyman-α probe measures more detail on nonlinear scales and can better constrain the DM particle mass (for example, see Refs. [69–73]). In particular, the current Lyman-α forest observations have excluded DM candidates with particle masses smaller than 5.3 keV [55] (we thank the anonymous referee for informing us of these new data), as their free-streaming lengths are too great. Explicitly, using Eq. (19), we find that EQFIDM candidates of types corresponding to negligible entropy production ($I \ll 1$: Type 1, Type 2, Type 3, and Type 4) have been excluded (one can also gain some intuition about how the Lyman-α observations can exclude certain cases from Fig. 3). On the other hand, EQFIDM candidates of types corresponding to significant entropy production ($I \gg 10^2$: Type 5, Type 7, and Type 8) are cold enough to be compatible with these observations. Meanwhile, Type 6 ($0 \leq I \ll \epsilon$, $\epsilon \gg 1$) requires $\epsilon \gg I \gg 10^2$ to be compatible with the current observations. Type 9, for which the EQFIDM particle mass is independent of ϵ, can also be compatible with the current observations in a sizeable parameter space of $\Gamma_\star/2H(t_{fi})$ and w_b, as we will show.

In Fig. 4, we plot the exclusion region ($m_\chi \leq 5.3$ keV) for Type 9 with respect to w_b and $\Gamma_\star/2H(t_{fi})$. As this figure shows, there is a sizeable region in which EQFIDM can be compatible with the current Lyman-α forest observations [55]. Specifically, in the outermost region (5.3 keV $\leq m_\chi \leq$ 100 keV), the EQFIDM is warm because the entropy production from the RBF is mild. However, in the inner regions, with very effective entropy production, the EQFIDM particle mass is very large and can even exceed the TeV scale. In these regions, the EQFIDM can be considered a CDM candidate, which is worthy of further study.

Furthermore, according to the above analysis, both Type 9 (for the outermost region) and Type 6 (with large ϵ) can serve as warm DM candidates. Therefore, we are motivated to investigate their potential to alleviate the well-known small-scale crisis (SSC). As one of the most critical outstanding puzzles in modern astrophysics, the SSC refers to an underlying discrepancy between cosmological predictions and astrophysical observations, which manifests in

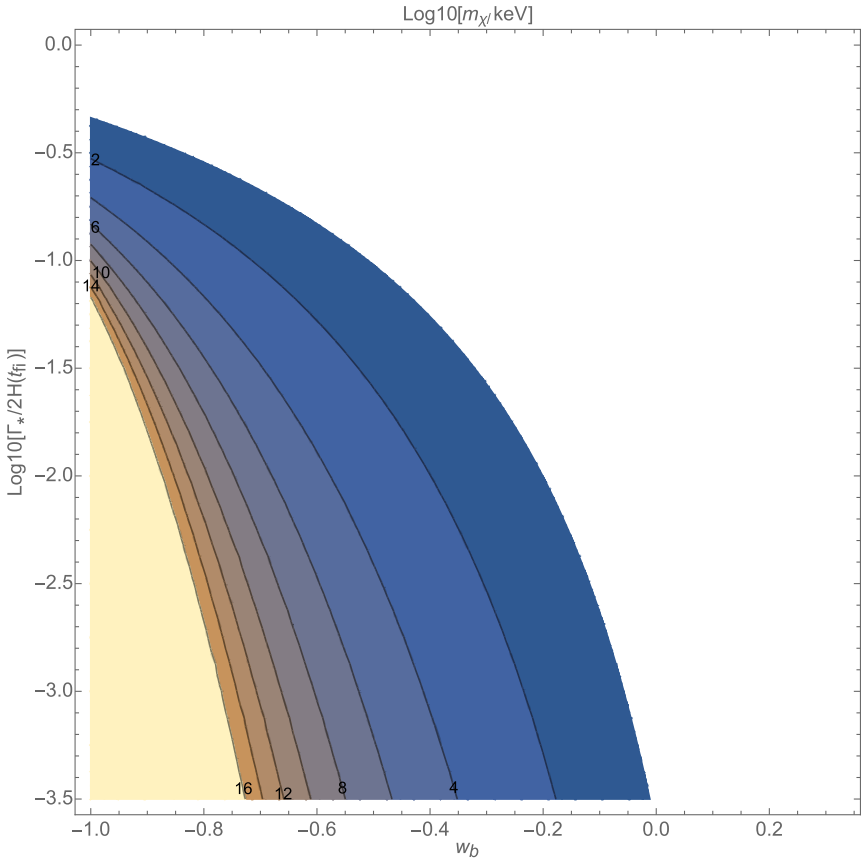

FIG. 4. Contour plot for the mass of EQFIDM particles of Type 9 with respect to the fundamental nature of the RBF, as characterized by w_b and $\Gamma_\star/2H(t_{fi})$. The blank region is excluded by the current Lyman-α forest observations.

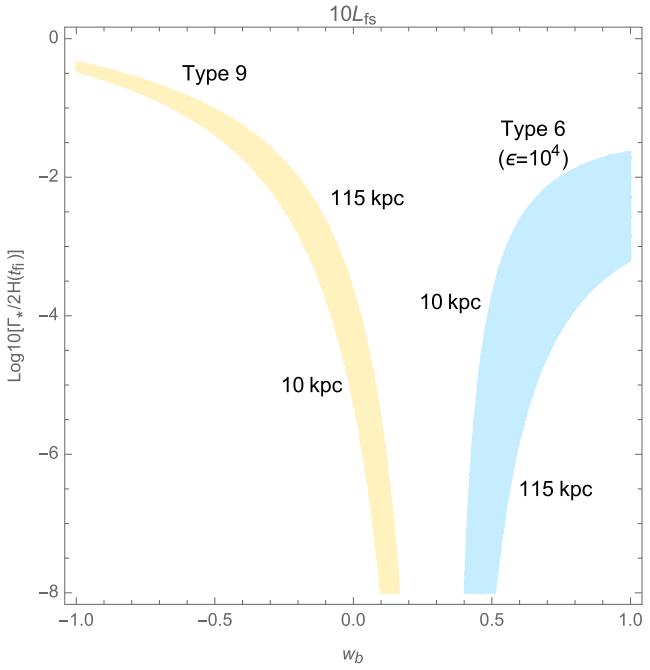

FIG. 5. Parameter regions for Type 9 and Type 6 (with $\epsilon = 10^4$) for 5.3 keV $\leq m_\chi \leq$ 32.6 keV in which the corresponding EQFIDM candidates can alleviate the SSC by inducing a suppression of the linear matter spectrum at 10 kpc $\leq 10L_{\rm fs} \leq$ 115 kpc.

three main aspects: *the missing satellites problem*, *the cusp vs core problem*, and *the too-big-to-fail problem* [57]. More specifically, current observations on the subgalactic scale indicate that fewer satellites are observed than are predicted from N-body numerical simulations based on standard ΛCDM cosmology. Additionally, the observed satellites are less concentrated than theoretically predicted. Although this crisis may be alleviated by the further elucidation of subtle baryonic physics and/or better interpretation of the observational data [74–80], it may also imply a suppression of the matter density perturbations at small scales (10 kpc $\leq l \leq$ 200 kpc) [56]. To realize such suppression, many salient mechanisms beyond simple inflation and CDM have been proposed, mainly including nonsimple-inflation-inspired models such as broken-scale-invariance inflation [81–84] and nonsimple-DM-inspired models such those presented in [85–92]. Warm DM candidates can also induce the desired suppression, as their motion can smooth out anisotropies and inhomogeneities at scales comparable to their free-streaming lengths [93–99].

In Fig. 5, we illustrate the parameter regions for Type 9 and Type 6 (with $\epsilon = 10^4$) for 5.3 keV $\leq m_\chi \leq$ 32.6 keV. These candidates can alleviate the SSC by inducing a suppression of the linear matter spectrum at 10 kpc $\leq 10L_{\rm fs} \leq$ 115 kpc in $(\Gamma_\star/2H(t_{fi}), w_b)$ space. As this figure shows, both types have sizeable parameter regions in which they can alleviate the SSC. The results for Type 9 imply that even though the RBF may contribute only a tiny portion of the total energy density at freeze-in and have only a very tiny decay rate, it can still alleviate the SSC. However, the remaining seven types of candidates cannot alleviate the SSC because their entropy production is either too efficient or too inefficient.

V. SUMMARY

In this paper, by carefully examining the thermal decoupling conditions within a generic bouncing universe, we reveal a new fermionic DM candidate called thermal equilibrium freeze-in DM (EQFIDM), which can freeze into thermal equilibrium shortly after a bounce. Because the relic abundance of EQFIDM depends on the post-freeze-in entropy production, we use it as a novel probe to trace the entropy production from the residual bouncing field (RBF). Specifically, we present a model-independent formalism to obtain all nine possible types of entropy-producing RBF decay processes within a generic bouncing cosmos (Type 1—Type 9). We find that due to the magnitudes of entropy production from these different types of processes, the EQFIDM particle mass can range from the sub-keV scale to the super-TeV scale.

Using current Lyman-α forest observations, we find that although four types of RBF decay processes (Type 1—Type 4) have already been excluded because of their low entropy production, the remaining five types, which suggest warm and cold EQFIDM candidates with efficient entropy production, are accommodated by the current observations, in either the whole parameter region (Type 5, Type 7, and Type 8) or some part of it (Type 6 and Type 9). In particular, for redominant entropy-producing RBF decay (Type 9), the entropy production is independent of the energy density ratio at freeze-in, ϵ, which implies that the EQFIDM particle mass in this case is determined solely by the fundamental nature of the RBF ($\Gamma_\star/2H(t_f i)$ and w_b). Then, we illustrate how the nature of the RBF can be constrained by the current observations.

Furthermore, because both Type 9 and Type 6 admit warm DM candidates within certain parts of their parameter regions, we also investigate their potential to alleviate the small-scale crisis (SSC). It turns out that both types of candidates have a sizeable parameter region that can alleviate the SSC. In particular, the results for Type 9 indicate that even though the RBF may contribute only a tiny portion of the total energy density at freeze-in and have only a very tiny decay rate, the SSC can still be alleviated.

In summary, our model-independent analysis may shed light on model building in bouncing cosmology. Through optimization based on future astrophysical observations, the entropy-producing decay processes of the RBF and the properties of different types of EQFIDM may be further constrained. In addition, it is hoped that the results for Type 9 may help us better understand the SSC in regard to postbounce entropy production. Finally, we wish to highlight that a similar analysis can also be applied to the

NEQDM candidate, as its abundance is also sensitive to the entropy-producing decay of the RBF.

ACKNOWLEDGMENTS

I thank Yeuk-Kwan Edna Cheung and Ligong Bian for the useful discussion. This work has been supported in parts by the National Natural Science Foundation of China (Grants No. 11963005, No. 11603018, No. 11775110, No. 11433004, No. 11690030), the Natural Science Foundation of Yunnan Province (Grants No. 2016FD006, No. 2015HA022, No. 2015HA030), and the Science & Technology Department of Yunnan Province - Yunnan University Joint Funding (Grant No. 2019FY003005).

APPENDIX: REDOMINANCE CONDITION

To ensure that the RBF is always subdominant for Type 1, we have $\rho_\gamma(t_{fi}+\Delta t) \gg \rho_b(t_{fi}+\Delta t)$, with $\Delta t = \Gamma_\star^{-1}$ being the half-life of the RBF, which leads to

$$\left(\frac{a(t_{fi})}{a(t_{fi}+\Gamma_\star^{-1})}\right)^{1-3w_b} \gg \epsilon, \tag{A1}$$

where $\epsilon \equiv \rho_b(t_{fi})/\rho_\gamma(t_{fi}) \ll 1$ for the subdominant case and the redominant case. By substituting Eq. (20) into this expression, we obtain

$$\Gamma_\star \gg 2H(t_{fi})[\epsilon^{-\frac{2}{1-3w_b}}-1]^{-1}, \tag{A2}$$

which is the subdominance condition for the RBF. Additionally, by applying this condition to Type I ($\Gamma_\star < 2H(t_{fi})$, $-1 \le w_b \le \frac{1}{3}$ and $\epsilon < 1$), we can obtain

$$\begin{aligned} I &\ll \epsilon \times \epsilon^{-1} e^{\frac{\Gamma_\star}{2H(t_{fi})}} \Gamma\left[\frac{3}{2}(1-w_b), \frac{\Gamma_\star}{2H(t_{fi})}\right] \\ &\simeq \Gamma\left[\frac{3}{2}(1-w_b)\right] \simeq 1, \end{aligned} \tag{A3}$$

where $\Gamma[n]$ is the Gamma function, which indicates that the entropy production for Type I is also negligible.

Accordingly, we can obtain the redominance condition for Type 9,

$$\Gamma_\star \ll 2H(t_{fi})[\epsilon^{-\frac{2}{1-3w_b}}-1]^{-1}, \tag{A4}$$

which straightforwardly leads to the following useful relation for Type 9:

$$\frac{\rho_b(t_{rd})}{\rho_b(t_{fi})}\left(\frac{a(t_{rd})}{a(t_{fi})}\right)^4 = e^{-\frac{\Gamma_\star}{2H(t_{fi})}(\epsilon^{-\frac{2}{1-3w_b}}-1)} \epsilon^{-\frac{2}{1-3w_b}\cdot\frac{1-3w_b}{2}} = \epsilon^{-1}. \tag{A5}$$

[1] A. H. Guth, Phys. Rev. D **23**, 347 (1981).
[2] V. F. Mukhanov, H. A. Feldman, and R. H. Brandenberger, Phys. Rep. **215**, 203 (1992).
[3] E. Komatsu *et al.* (WMAP Collaboration), Astrophys. J. Suppl. **192**, 18 (2011).
[4] P. A. R. Ade *et al.* (Planck Collaboration), Astron. Astrophys. **594**, A13 (2016).
[5] A. Borde and A. Vilenkin, Phys. Rev. Lett. **72**, 3305 (1994).
[6] J. Khoury, B. A. Ovrut, P. J. Steinhardt, and N. Turok, Phys. Rev. D **64**, 123522 (2001).
[7] M. Gasperini and G. Veneziano, Phys. Rep. **373**, 1 (2003).
[8] P. Creminelli, M. A. Luty, A. Nicolis, and L. Senatore, J. High Energy Phys. 12 (2006) 080.
[9] P. Peter, E. J. C. Pinho, and N. Pinto-Neto, Phys. Rev. D **75**, 023516 (2007).
[10] Y. F. Cai, T. Qiu, Y. S. Piao, M. Li, and X. Zhang, J. High Energy Phys. 10 (2007) 071.
[11] Y. F. Cai, T. t. Qiu, R. Brandenberger, and X. m. Zhang, Phys. Rev. D **80**, 023511 (2009).
[12] T. Saidov and A. Zhuk, Phys. Rev. D **81**, 124002 (2010).
[13] C. Li, L. Wang, and Y. K. E. Cheung, Phys. Dark Universe **3**, 18 (2014).
[14] Y. F. Cai, S. H. Chen, J. B. Dent, S. Dutta, and E. N. Saridakis, Classical Quantum Gravity **28**, 215011 (2011).
[15] D. A. Easson, I. Sawicki, and A. Vikman, J. Cosmol. Astropart. Phys. 11 (2011) 021.
[16] K. Bhattacharya, Y. F. Cai, and S. Das, Phys. Rev. D **87**, 083511 (2013).
[17] T. Qiu and Y. T. Wang, J. High Energy Phys. 04 (2015) 130.
[18] Y. F. Cai, A. Marciano, D. G. Wang, and E. Wilson-Ewing, Universe **3**, 1 (2017).
[19] J. D. Barrow and C. Ganguly, Phys. Rev. D **95**, 083515 (2017).
[20] J. De Haro and J. Amors, Phys. Rev. D **97**, 064014 (2018).
[21] A. Ijjas and P. J. Steinhardt, Classical Quantum Gravity **35**, 135004 (2018).
[22] S. S. Boruah, H. J. Kim, M. Rouben, and G. Geshnizjani, J. Cosmol. Astropart. Phys. 08 (2018) 031.
[23] S. Nojiri, S. D. Odintsov, and E. N. Saridakis, Nucl. Phys. **B949**, 114790 (2019).
[24] M. Novello and S. E. P. Bergliaffa, Phys. Rep. **463**, 127 (2008).
[25] R. Brandenberger and P. Peter, Found. Phys. **47**, 797 (2017).
[26] S. Nojiri, S. D. Odintsov, and V. K. Oikonomou, Phys. Rep. **692**, 1 (2017).
[27] D. Wands, Phys. Rev. D **60**, 023507 (1999).

[28] F. Finelli and R. Brandenberger, Phys. Rev. D **65**, 103522 (2002).
[29] L. A. Boyle, P. J. Steinhardt, and N. Turok, Phys. Rev. D **70**, 023504 (2004).
[30] C. Li and Y. K. E. Cheung, J. Cosmol. Astropart. Phys. 07 (2014) 008.
[31] Y. F. Cai, W. Xue, R. Brandenberger, and X. m. Zhang, J. Cosmol. Astropart. Phys. 06 (2009) 037.
[32] X. Gao, M. Lilley, and P. Peter, Phys. Rev. D **91**, 023516 (2015).
[33] I. Ben-Dayan, J. Cosmol. Astropart. Phys. 09 (2016) 017.
[34] D. C. F. Celani, N. Pinto-Neto, and S. D. P. Vitenti, Phys. Rev. D **95**, 023523 (2017).
[35] T. Clifton, B. Carr, and A. Coley, Classical Quantum Gravity **34**, 135005 (2017).
[36] S. Ni, H. Li, T. Qiu, W. Zheng, and X. Zhang, Eur. Phys. J. C **78**, 608 (2018).
[37] X. Chen, A. Loeb, and Z. Z. Xianyu, Phys. Rev. Lett. **122**, 121301 (2019).
[38] N. Zhang and Y. K. E. Cheung, Eur. Phys. J. C **80**, 100 (2020).
[39] E. Elizalde, S. D. Odintsov, V. K. Oikonomou, and T. Paul, Nucl. Phys. **B954**, 114984 (2020).
[40] E. Frion, N. Pinto-Neto, S. D. P. Vitenti, and S. E. P. Bergliaffa, Phys. Rev. D **101**, 103503 (2020).
[41] L. L. Graef, R. O. Ramos, and G. S. Vicente, Phys. Rev. D **102**, 043518 (2020).
[42] C. Li, R. H. Brandenberger, and Y. K. E. Cheung, Phys. Rev. D **90**, 123535 (2014).
[43] B. W. Lee and S. Weinberg, Phys. Rev. Lett. **39**, 165 (1977).
[44] G. Steigman and M. S. Turner, Nucl. Phys. **B253**, 375 (1985).
[45] S. Dodelson and L. M. Widrow, Phys. Rev. Lett. **72**, 17 (1994).
[46] D. J. H. Chung, E. W. Kolb, and A. Riotto, Phys. Rev. Lett. **81**, 4048 (1998).
[47] X. D. Shi and G. M. Fuller, Phys. Rev. Lett. **82**, 2832 (1999).
[48] J. L. Feng, A. Rajaraman, and F. Takayama, Phys. Rev. Lett. **91**, 011302 (2003).
[49] L. J. Hall, K. Jedamzik, J. March-Russell, and S. M. West, J. High Energy Phys. 03 (2010) 080.
[50] M. Klasen and C. E. Yaguna, J. Cosmol. Astropart. Phys. 11 (2013) 039.
[51] B. Feldstein, M. Ibe, and T. T. Yanagida, Phys. Rev. Lett. **112**, 101301 (2014).
[52] H. Baer, K. Y. Choi, J. E. Kim, and L. Roszkowski, Phys. Rep. **555**, 1 (2015).
[53] Y. K. E. Cheung, J. U. Kang, and C. Li, J. Cosmol. Astropart. Phys. 11 (2014) 001.
[54] C. Li, Phys. Rev. D **92**, 063513 (2015).
[55] V. Iršič, M. Viel, M. G. Haehnelt, J. S. Bolton, S. Cristiani, G. Cupani, T. S. Kim, V. D'Odorico, S. López, and S. Ellison *et al.*, Phys. Rev. D **96**, 023522 (2017).
[56] K. Markovic and M. Viel, Pub. Astron. Soc. Aust. **31**, e006 (2014).
[57] D. H. Weinberg, J. S. Bullock, F. Governato, R. K. de Naray, and A. H. G. Peter, Proc. Natl. Acad. Sci. U.S.A. **112**, 12249 (2015).
[58] Y. F. Cai, R. Brandenberger, and X. Zhang, Phys. Lett. B **703**, 25 (2011).
[59] NEQDM continues to be produced during the bounce phase because it has not reached thermal equilibrium, so its matching condition should be $Y^+(T_{\rm max}) = Y^-(T_{\rm max})$, where $T_{\rm max}$ is the background temperature when the universe reaches its minimum size $a_{\rm min}$. For an efficient bounce, we have $a_{\rm min} \sim a(T_b)$ and $T_b \sim T_{\rm max}$, which can also lead to $Y^+(T_b) = Y^-(T_b)$. Only if the bounce is not efficient, $T_b \ll T_{\rm max}$, should such a correction be taken into account for NEQDM. In this paper, because we mainly focus on EQFIDM, we use $Y^+(T_b) = Y^-(T_b)$ for all three candidates in our calculation for simplicity.
[60] P. Gondolo and G. Gelmini, Nucl. Phys. **B360**, 145 (1991).
[61] Before $y = 1$, the background temperature is less than the DM particle mass, so no DM particle can be thermally produced, i.e., $Y_- = 0$ for $y \geq 1$. Thus, we can use $Y_-(y = 1) = 0$ as the initial condition.
[62] In the high-temperature bounce scenario, the (possible) domination and entropy-producing decay of the RBF occur much earlier than the annihilation of SM particles, which happens between 100 GeV and 1 MeV. Given these considerations, we can choose $T_r \sim 100$ GeV (or a higher energy scale) to separate RBF decay from SM particles annihilation. Furthermore, as its energy scale ($\gg$100 GeV) is also much higher than the big bang nucleosynthesis (BBN) ($\leq$10 MeV), the RBF decay also does not disturb BBN or other processes occurring after BBN. Consequently, it is also free from the cosmological constraints on post-BBN processes, such as nonradiation energy density components and post-BBN entropy injection. Note that, if there were to be more cosmological constraints from other (forthcoming) observations that could be imposed on this new model, this would be very encouraging and worthy of further study. Thank the anonymous referee for noting this point.
[63] S. Dodelson, *Modern Cosmology* (Academic Press, Amsterdam, 2003).
[64] A. Boyarsky, O. Ruchayskiy, and D. Iakubovskyi, J. Cosmol. Astropart. Phys. 03 (2009) 005.
[65] Y. F. Cai, E. N. Saridakis, M. R. Setare, and J. Q. Xia, Phys. Rep. **493**, 1 (2010).
[66] E. A. Baltz and H. Murayama, J. High Energy Phys. 05 (2003) 067.
[67] A. R. Zentner and J. S. Bullock, Astrophys. J. **598**, 49 (2003).
[68] S. Weinberg, *Cosmology* (Oxford University Press, Oxford, 2008).
[69] V. Iršič, M. Viel, M. G. Haehnelt, J. S. Bolton, and G. D. Becker, Phys. Rev. Lett. **119**, 031302 (2017).
[70] A. Garzilli, A. Magalich, T. Theuns, C. S. Frenk, C. Weniger, O. Ruchayskiy, and A. Boyarsky, Mon. Not. R. Astron. Soc. **489**, 3456 (2019).
[71] M. Nori, R. Murgia, V. Iršič, M. Baldi, and M. Viel, Mon. Not. R. Astron. Soc. **482**, 3227 (2019).
[72] S. Bose, M. Vogelsberger, J. Zavala, C. Pfrommer, F. Y. Cyr-Racine, S. Bohr, and T. Bringmann, Mon. Not. R. Astron. Soc. **487**, 522 (2019).
[73] A. Kamada and K. Yanagi, J. Cosmol. Astropart. Phys. 11 (2019) 029.
[74] J. D. Simon and M. Geha, Astrophys. J. **670**, 313 (2007).

[75] J. Diemand, M. Kuhlen, P. Madau, M. Zemp, B. Moore, D. Potter, and J. Stadel, Nature (London) **454**, 735 (2008).
[76] M. Ackermann *et al.* (Fermi-LAT Collaboration), Phys. Rev. Lett. **107**, 241302 (2011).
[77] L. Amendola *et al.* (Euclid Theory Working Group), Living Rev. Relativity **16**, 6 (2013).
[78] S. E. Koposov, V. Belokurov, G. Torrealba, and N. W. Evans, Astrophys. J. **805**, 130 (2015).
[79] A. Drlica-Wagner *et al.* (Fermi-LAT and DES Collaborations), Astrophys. J. Lett. **809**, L4 (2015).
[80] S. Y. Kim, A. H. G. Peter, and J. R. Hargis, Phys. Rev. Lett. **121**, 211302 (2018).
[81] M. Kamionkowski and A. R. Liddle, Phys. Rev. Lett. **84**, 4525 (2000).
[82] J. Yokoyama, Phys. Rev. D **62**, 123509 (2000).
[83] T. Kobayashi and F. Takahashi, J. Cosmol. Astropart. Phys. 01 (2011) 026.
[84] T. Nakama, J. Chluba, and M. Kamionkowski, Phys. Rev. D **95**, 121302 (2017).
[85] W. B. Lin, D. H. Huang, X. Zhang, and R. H. Brandenberger, Phys. Rev. Lett. **86**, 954 (2001).
[86] K. Sigurdson and M. Kamionkowski, Phys. Rev. Lett. **92**, 171302 (2004).
[87] A. Kusenko, Phys. Rep. **481**, 1 (2009).
[88] M. Rocha, A. H. G. Peter, J. S. Bullock, M. Kaplinghat, S. Garrison-Kimmel, J. Onorbe, and L. A. Moustakas, Mon. Not. R. Astron. Soc. **430**, 81 (2013).
[89] Y. Hochberg, E. Kuflik, T. Volansky, and J. G. Wacker, Phys. Rev. Lett. **113**, 171301 (2014).
[90] R. Foot and S. Vagnozzi, Phys. Rev. D **91**, 023512 (2015).
[91] Y. Hochberg, E. Kuflik, H. Murayama, T. Volansky, and J. G. Wacker, Phys. Rev. Lett. **115**, 021301 (2015).
[92] S. Tulin and H. B. Yu, Phys. Rep. **730**, 1 (2018).
[93] P. Bode, J. P. Ostriker, and N. Turok, Astrophys. J. **556**, 93 (2001).
[94] P. Colin, V. Avila-Reese, and O. Valenzuela, Astrophys. J. **542**, 622 (2000).
[95] M. Viel, K. Markovic, M. Baldi, and J. Weller, Mon. Not. R. Astron. Soc. **421**, 50 (2012).
[96] A. V. Maccio, O. Ruchayskiy, A. Boyarsky, and J. C. Munoz-Cuartas, Mon. Not. R. Astron. Soc. **428**, 882 (2013).
[97] M. Viel, G. D. Becker, J. S. Bolton, and M. G. Haehnelt, Phys. Rev. D **88**, 043502 (2013).
[98] R. Murgia, A. Merle, M. Viel, M. Totzauer, and A. Schneider, J. Cosmol. Astropart. Phys. 11 (2017) 046.
[99] S. Kumar, R. C. Nunes, and S. K. Yadav, Mon. Not. R. Astron. Soc. **490**, 1406 (2019).